Journal of Theoretical and Applied Information Technology
15th April 2022. Vol.100. No 7

ISSN: 1992-8645 www.jatit.org E-ISSN: 1817-3195

MULTI-OBJECTIVE RIDER BASED ELEPHANT HERD OPTIMIZATION FOR SPECTRAL UNMIXING OF HYPERSPECTRAL IMAGES

[1] RAJA NATARAJAN, [2] VADIVEL RAMASAMY
[1]Ph.D. Scholar, Department of Information Technology, Bharathiar University, Coimbatore, India
Assistant Professor (Computer Science), Tamil Nadu Agricultural University, Coimbatore, India
[2]Assistant Professor, Department of Information Technology, Bharathiar University, Coimbatore,
E-mail: [1]nraja@tnau.ac.in, [2]vlr_vadivel@yahoo.co.in

ABSTRACT

Spectral unmixing (SU) is used for the identification of the end members and fractional abundances present in the mixed pixels of the hyperspectral images that are rich in data. The traditional methods for spectral unmixing are affected with the artifacts requiring the effective method for spectral unmixing. Thus, the paper uses an effective framework for Spectral unmixing using the proposed Rider based Elephant Herd Optimization (R-EHO). The proposed Rider based Elephant Herd Optimization estimates the fractional abundance using the end members and proposed Rider based Elephant Herd Optimization is the integration of the standard Elephant Herd optimization (EHO) in the Rider Optimization algorithm (ROA). The proposed optimization uses the multi-objective function that is modelled using the factors, such as Reconstruction Error (RSE), sparsity (SPA), spatial neighbor (SNI), and spatial neighbour correlation (SNC), and mutual information. The analysis is progressed using the Urban and Cuprite datasets based on the performance metrics, Root-Mean-Square Error (RMSE), Reconstruction Error (RE) and it is proved that the proposed R-EHO acquired the minimal RE and minimal RMSE of 13.8576 and 0.0011, respectively.

Keywords: *Optimization, Spectral Unmixing, Hyperspectral Images, End Components, Fractional Abundances*

1. INTRODUCTION

Hyperspectral imagery is attracting both in the civilian and military applications as the hyperspectral image consists of a huge amount of information regarding the latent components in the individual pixel [9]. Hyperspectral images are rich in the spatial information, which benefits the estimation of the endmember abundances and thereby, enabling the consistency of the obtained abundances [1]. Hyperspectral imagery captures same scene from a number of contiguous spectral bands, such as visible, near and shortwave infrared bands, which are used in a vast range of applications, like detection and exploration of minerals, terrain classification, discrimination of the military target, monitoring the environment, and counterfeiting the pharmaceutics [12]. Hyperspectral imaging sensors are employed to compute the energy corresponding to the received light with respect to tens and hundreds of narrow spectral bands in individual spatial position of the image [11]. Thus, the individual pixel is presented as a high-dimensional vector along the dimensions of the wavelength, termed as the spectrum belonging to the material present in that particular pixel [10]. However, the inability of the hyperspectral sensors with less spatial resolution, the pixels in the image are often mixed representing the homogeneous mix of distinct components [14] [9]. The presence of the mixed pixels badly affects the application of the hyperspectral data [15]. Thus, spectral unmixing is required for exploiting the detailed data regarding the properties of the components in the individual pixel of the scene [9].

The deep breath about the spectral unmixing process is a significant condition of the generalized inverse issue, which estimates parameters corresponding to an object based on the observation of a signal that had the interaction with the object prior to the arrival at the sensor [14][16]. Spectral unmixing is a significant technique for interpretation of the remotely sensed hyperspectral image, for decomposing the image as a set of pure spectral endmembers along with their abundance fractions with respect to the individual pixel of the scene [1]. Spectral unmixing estimates the fractional abundances corresponding to the pure

signatures of spectrum or end members corresponding to the individual mixed pixel, and the issue is regarding the mixing issue [1]. Sparse unmixing estimates few endmembers available in a specific spectral library, representing the individual mixed pixel of the hyperspectral scene [3]. For enhancing the outcome of unmixing, there is a recent evolution for exploiting the spatial contextual information [1]. Sparse unmixing smoothen the textures and preserves the sharp edges available while estimating the abundance [1]. Sparse-representation-based methods are used widely for remotely sensed hyperspectral unmixing [1] and the algorithms used specifically depends on the expected mixing type that is either classified as linear or nonlinear model [15][21] . Nonlinear mixing model considers that a part of source radiation is exaggerated using the effects of multiple scattering through the usage of numerous endmembers in the scene prior to the collection at the sensor. Thus, the spectrum observed using the mixed pixel is obtained using the nonlinear function of abundance corresponding to the endmembers [15].

Linear mixture model (LMM) considers that mixing occurs within a measuring instrument and in addition takes into-account the interactions existing between the distinct endmembers that are negligible. Therefore, the observed spectrum of mixed pixel is uttered as a linear combination end member signatures that are weighted with their corresponding fractional abundances [15]. LMM resembles a precise model for characterizing a number of the real scenarios and it is recognized as the acceptable approximation of instrument mechanism and light scattering [15]. LMM is employed for HU as a result of the simplicity and effectiveness in numerous applications along with the computational tractability. Depending on LMM, there are many methods, like geometry and statistics dependent approaches [15] [17]. Methods based on geometry deploy the pixel observations of the hyperspectral data that are within the simplex and vertices with respect to the endmember. The methods include vertex component analysis [20], N-FINDR [18], simplex growing algorithm [23], minimum-volume simplex analysis [22], and so on [15]. Statistical approaches use the statistical characteristic belonging to the hyperspectral data, like Nonnegative Matrix Factorization (NMF) and Independent Component Analysis (ICA) [24] [15] [13]. Generally, the methods estimate the endmembers or determine the availability of pure pixels. The assumptions do not hold for most of the hyperspectral data and the availability of the mixture at various scales [15]. A simple method to manage the spatial and spectral features is vector stacking that combines variety of features as a long vector. However, unfortunately, stacking the spectral and spatial feature may generate a feature vector of higher dimensional [26] [27].

The primary intention of this research is to design and develop a a novel approach for the spectral unmixing with the hyperspectral satellite image by proposing an optimization algorithm. Here, a novel optimization algorithm, named R-EHO, is developed considering various objectives. The proposed R-EHO is used for estimating the fractional abundance of every end member by considering a non-linear sparse unmixing model. The proposed R-EHO algorithm is designed by the integration of ROA [29] and EHO [28] by making use of multiple objectives to optimize the reconstruction, sparsity and the total variation regularization terms concurrently. Here, a new objective function is developed by considering five objectives, namely RSE, SPA, SNI, SNC, and mutual information. This objective function is utilized to estimate the fractional abundance of end member for unmixing.

1.1 Research Objectives

The following research objectives are formlated to address the hyperspectral unmixing problem.

i. To characterize the hyperspectral images with the multi-objective sparse hyperspectral unmixing optimization variables.
ii. To estimate the fractional abundances, extract the pure pixels and compare with the spectral library of the hyperspectral image.
iii. To evaluate and compare the performance of the multi-objective sparse spectral unmixing techniques and identify the efficient spectral unmixing approach.

1.2 Research Contribution from the Proposed Work

The proposed research work of R-EHO contributes in various applications areas such as remote sensing, audio signal processing, and chemistry. Hyperspectral imaging (HSI) are known to have low spatial resolution despite their great spectral resolution. The low spatial resolution despite their great spectral resolution would made the HSI pixel

values to be a combination of different materials in the picture. Hyperspectral Unmixing may thus be dismissed as an inverse technique that involves determining the amount of pure elements contributing to the pixels' mixture in each pixel. The overall number of pure elements (also known as endmembers) and the number of them included in a single pixel are two data points that are difficult to get. When both the total number and kind of endmembers in the scene are known and connected with a linear mixing process assumption, the situation is the simplest. This linearity assumption, while useful in some cases, does not hold in most real-world scenarios. In most circumstances, knowledge of a material's endmember signature isn't exact, necessitating the need to account for differences across different representations of the same material. Last but not least, the presence of abnormalities and noise is a common problem that affects estimation accuracy. The aforementioned challenges were primarily brought to light in this work, and answers to these open problems were supplied by introducing an evolutionary multi-objective R-EHO optimization algorithm.

The fractional abundance of the end members is determined optimally using the proposed R-EHO algorithm, which is the integration of EHO and ROA. The optimization algorithm, R-EHO exhibits the higher local convergence avoidance and global convergence when compared with the other optimizations and in addition, the diversity during search is increased.

1.3 Objective Function

The objective function is formulated based on the multi-objective constraints, such as RSE, SPA, SNI, and SNC along with the mutual information in such a way that the proposed R-EHO uses the objective function to estimate the end members.

The organization of the paper is: section 1 demonstrates the background of spectral unmixing and the methods existing in the literature are discussed in section 2 along with the challenges of the method. The proposed method of unmixing is discussed in section 3 and section 4 presents the results of the method. Finally, section 5 concludes the paper.

2. REVIEW OF LITERATURE

In this section, eight literature methods are reviewed. Shaoquan Zhang ,et al [1] developed a Spatial discontinuity weighted sparse unmixing approach for accurately preserving the boundaries of the image. The method lacked the ability to preserve the heterogeneity of abundance maps. Xiangming Jiang, et al [2] modelled a decomposition algorithm, named endmember selection algorithm, which minimized the residuals of image unmixing that achieved the higher visual quality. The method achieved the better unmixig performance even in the presence of noises and interferences. The drawback of the method was that the method failed for implementing the two-phase multiobjective sparse unmixing (Tp-MoSU) in parallel way for utilizing the multiobjective optimization. Dan Wang, et al. [3] developed a method based on the sparse redundant unmixing algorithm that attained the higher performance in unmixing. The drawback of the method was that the method failed to regularize the total variation (TV) of redundant spectra. Burkni Palsson, et al. [4] developed a model, linear mixture that exhibited the higher degree of robustness to noise. The spectral resolution was high with minimal cost and it was easy for utilizing the custom objective function. The method failed in utilizing the symmetrical architecture with tied weights for decoder and encoder. Maoguo Gong, et al. [5] modelled a Multi-objective cooperative coevolutionary algorithm that directly optimized the non-convex model in generating the non-dominated solution set with a single run. The failure of the method was that the method failed to utilize the spatial information. Yanli Sun, et al. [6] modelled an approach named as Class-based endmember extraction and sparse Unmixing approach that enhanced the classification performance of semisupervised model with higher accuracy. The drawback of the method was regarding the usage of the spatial information of the spectrum in addition to the abundance information. Rui Wang, et al. [7] used the double reweighted sparse unmixing and total variation algorithm, which enhanced the performance of unmixing and along with that the data sparsity of the fractional abundances was enhanced. The failure of the method was regarding the selection of the adaptive parameter. Rui Wang, et al. [8] used a Centralized collaborative sparse unmixing (CCSU) algorithm that reduced the estimation error, but the method failed to automatically update the regularization parameters. The multi-fidelity evolutionary multitasking optimization (MFEMO) framework [33] framework is presented to address the issues in endmember extraction caused by outliers and expensive computation. MFEMO, on

the other hand, incorporates unavoidable negative transfer across tasks during endmember extraction, which degrades endmember estimation accuracy]. An evolutionary multi-objective hyperspectral sparse unmixing algorithm is developed with endmember priori approach to deal with large-scale sparse unmixing difficulties (EMSU-EP). It's tough to control noise in large-scale sparse unmixing problems with this approach[34]. A multiobjective-based simultaneous sparse unmixing framework (PMoSU), which includes three concurrent objectives for spectral unmixing in high-noise environments: reconstruction error, sparsity error, and the pruning projection function. Weakly Pareto optimal solutions may emerge in the situation of discrete range sparse unmixing [35].

2.1 Research Challenges

The challenges of the research are enlisted below:

- Decomposition based end member selection algorithm [2] is used for solving the two-phase multi-objective issue that required weights both for the encoder and decoder. It comprises of the unmixing residuals and active end members, to determine the real end members that are active. However, for experiencing the merits of multi-objective optimization, there is a need to implement the Tp-MoSU in parallelly, which is a major shortcoming of the method.
- Augmented Lagrangian algorithm [12] is used for dealing with the low complexity problem in unmixing and Compressive Sensing (CS) method. A device captures the compressed hyperspectral data as like the single-pixel camera and decodes the compressed data to compute the unmixed abundance fractions directly for the given end members. The method fails in solving the models of non convex matrix factorization.
- Vertex Component Analysis (VCA) algorithm [17] is used to extract the unsupervised end member using the hyperspectral data. VCA iteratively places the data onto a direction in such a way it is orthogonal to the subspace spanned by the end members that are determined already. Though the computational complexity is lower, there is a problem when a large data set is used.
- Spatial-Spectral Pre processing (SSPP) methods are employed to identify the end member and spectral unmixing. A spatial homogeneity index is derived for the individual pixel present in the hyperspectral image, which is relatively insensitive to the noise available in the data [25]. Under the formulation of the current spectral and spatial data, there are cases that penalize the selection of anomalous endmembers.
- Sparse unmixing [19] using the variable splitting augmented Lagrangian concentrates on the hyperspectral data analyzing without using the spatial information. The shortcoming of the method was regarding the failure in establishing the fast parallel processing and regarding the high computational complexity.
- Hyperspectral Unmixing uses Robust Collaborative Nonnegative Matrix Factorization (R-CoNMF) method [26] to estimate the number of endmembers, the mixing matrix and the corresponding abundances but the algorithm is not evaluated using real hyperspectral datasets.
- In Multi objective optimization based sparse unmixing algorithm (MOSU) [32], the performance was found to be better in solving the sparse unmixing problem. The main drawback of the method was that the lack of the population-based algorithm, which is used to enhance the computation efficiency.

3. PROPOSED RIDER-ELEPHANT HERD OPTIMIZATION ALGORITHM

The proposed R-EHO algorithm is the integration of the EHO algorithm in the ROA in such a way that the update rule of bypass rider is modified using the update equation of EHO. The proposed R-EHO balances the merits and demerits of EHO and ROA and more importantly, the proposed algorithm renders a higher convergence rate with a global optimal solution and higher tendency towards the local optimal avoidance mechanism. On the other hand, the diversity of the solutions is assured with a better convergence rates and the capacity of R-EHO to deal with the multiple objectives is effective.

Basically, the standard ROA is developed based on the fictional computing concept, which is based on the imaginary thoughts and ideas unlike the other artificial computing algorithms and nature-inspired algorithms. ROA is duly based on the riding behaviour of the riders, such as bypass, follower, overtaker and attacker, and these riders possess the single objective of reaching the destination. Each of the riders takes their own way of riding to reach the destination and it is clear from the literature that ROA is the only algorithm functioning based on the imaginary ideas. Inspired with the behaviours of four groups of riders, ROA renders a global optimal solution. The evaluation factor is termed as the success rate that decides the leading rider based on which the other riders update their position in reaching the destination. The position update of the individual riders is based on the riding characteristics of the riders' vehicle, such as the steering angle, gear, accelerator, and so on. The position of the individual rider is accelerated towards the leading rider and the local minimal avoidance is discarded using the small local neighbourhood and this local optimal avoidance is the effort of the attacker. However, the higher convergence rate is based on the large global neighbors, which is handled using the overtaker. Thus, initially the riders explore the surroundings randomly for reaching the destination. The overtaker determines the optimal search space based on the success rate and directional indicator and the follower employs the multi-dimensional space in the leading rider. On the other hand, the searching speed of the attacker is accelerated based on the multidimensional search in addition to the fast search.

Similarly, EHO is inspired with the social behaviour of the elephants living in the clans and the elephants from different clans live together under the matriarch and the male elephants leave the group when they grow. EHO solves the optimization problem through two types of optimization operators, such as separating operator and clan updating operator. The position update of the elephants in the clan is based on the clan updating operator and the separating operator, enables the replacement of the worst elephant. Thus, the optimal convergence of EHO is better when compared with the other types of optimizations. The algorithmic steps of the proposed R-EHO algorithm are demonstrated below:

3.1 Rider Initialization

In this first step, the total riders in the search space are initialized and their positions are notated as,

$$R_{k,l}(t+1);(1\le k\le N);(1\le l\le z) \quad (1)$$

Where, N is the riders present in the search space and z refers to the total coordinates or dimension. $R_{k,l}(t)$ Denotes the position of k^{th} rider at time τ and the four rider groups are: bypass, attacker, overtaker, and follower are denoted as, R_1, R_3, R_2, and R_4. The riders taking part in the race are chosen equally from the individual rider groups as each group of riders hold specific riding specifications. The bypassing ability of the bypass rider, following the leader for updating the position of follower and attacker, and the self effort of attacker to reach the destination, are the overall characteristics of the rider groups. It is evident that the objectives of the individual rider groups are attained through varying the vehicle characteristics of the corresponding riders' vehicles. The riding parameters of k^{th} rider are: steering angle, coordinate angle, and position angle, which is notated as, $S_{k,l}(t)$, $C_{k,l}(t)$, and $P_{k,l}(t)$. Similarly, the gear, accelerator, and brake of k^{th} rider is represented as, G_k, A_k, and B_k, respectively. The gear κ_g value lies between 0 and 4, while the values of A_k, and B_k varies between 0 and 1.

3.2 Evaluating the Success Rate

The success rate decides the leading rider for which the success rate is maximal and the success rate is formulated based on the multi-objective function. The success rate is denoted as, SR and is otherwise termed as the multi-objective function.

3.3 Position Update for the Leading Rider

The leading rider is the one near to the destination and the declaration is made based on the maximal success rate. Until the off-time, the position of the rider is updated as the leading rider never is the same all the time.

3.4 Update Phase of the Rider Groups

The riders update their position based on the position of the leading rider and the position is modelled as follows:

3.4.1 Position of bypass rider

The position of the bypass rider is updated based on the position of the leader as given as,

$$R_{k,l}^{1}(t+1)=\alpha\left[R_{dk}(t)*\lambda(k)+R_{g,k}(t)*(1-\lambda(k))\right] \quad (2)$$

where, α is a random number varying between 0 and 1, d is the random number acquiring the values between 1 and N, λ is a random value between 0 and 1, and g takes a random value between 1 and N. The size of λ is denoted as, $(1 \times z)$, where z specifies the dimension of the total coordinates. Equation (2) is modified using the update rule of EHO algorithm in which the diversity of the solutions is enhanced. The update equation of EHO is given as,

$$R_{k,l}^{1}(t+1) = R_{k,l}(t) + \beta \times \left(R_{k}^{\text{best}} - R_{k,l}(t)\right) \times \varepsilon \quad (3)$$

where, $\beta \in [0, 1]$ refers to the scale factor and $R_{k,l}^{1}(t+1)$ indicates the updated position of l^{th} elephant in k^{th} clan, $R_{k,l}(t)$ is the previous position of l^{th} elephant in clan k. The random number ε varies in $[0, 1]$. Rearranging the equation (3) as given as,

$$R_{k,l}^{1}(t+1)=R_{k,l}(t)+\beta\times R_{k}^{best}\times\varepsilon-\beta\times R_{k,l}(t)\times\varepsilon \quad (4)$$

$$R_{k,l}^{1}(t+1)=R_{k,l}(t)[1-\beta\times\varepsilon]+\beta\times R_{k}^{best}\times\varepsilon \quad (5)$$

$$R_{k,l}(t)=\frac{R_{k,l}^{1}(t+1)-\beta\times R_{k}^{best}\times\varepsilon}{[1-\beta\times\varepsilon]} \quad (6)$$

Substitute eqn. (6) in eqn.(2) as,

$$R_{k,l}^{1}(t+1)=\alpha\left[\frac{R_{k,l}^{1}(t+1)-\beta\times R_{k}^{best}\times\varepsilon}{[1-\beta\times\varepsilon]}*\lambda(k)+R_{g,k}(t)*(1-\lambda(k))\right] \quad (7)$$

$$R_{k,l}^{1}(t+1)\frac{R_{k,l}^{1}(t+1)\times\alpha}{[1-\beta\times\varepsilon]}=\alpha\left[\frac{-\beta\times R_{k}^{best}\times\varepsilon}{[1-\beta\times\varepsilon]}*\lambda(k)+R_{g,k}(t)*(1-\lambda(k))\right] \quad (8)$$

$$R_{k,l}^{1}(t+1)\left[1-\frac{\alpha}{[1-\beta\times\varepsilon]}\right]=\alpha\left[R_{g,k}(t)*(1-\lambda(k))-\frac{\beta\times R_{k}^{best}\times\varepsilon}{[1-\beta\times\varepsilon]}*\lambda(k)\right] \quad (9)$$

$$R_{k,l}^{1}(t+1)\left[\frac{[1-\beta\times\varepsilon]-\alpha}{[1-\beta\times\varepsilon]}\right]=\alpha\left[R_{g,k}(t)*(1-\lambda(k))-\frac{\beta\times R_{k}^{best}\times\varepsilon}{[1-\beta\times\varepsilon]}*\lambda(k)\right] \quad (10)$$

$$R_{k,l}^{1}(t+1)=\frac{1-\beta\times\varepsilon}{[1-\beta\times\varepsilon]-\alpha}\left\{\alpha\left[R_{g,k}(t)*(1-\lambda(k))-\frac{\beta\times R_{k}^{best}\times\varepsilon}{[1-\beta\times\varepsilon]}*\lambda(k)\right]\right\} \quad (11)$$

Equation (11) is the modified equation of ROA, representing the update equation of R-EHO algorithm. The equation (11) reveals that the position of the rider is updated based on the riders' position in the previous iteration, random numbers, and best position of the rider.

3.4.2 Position of follower rider

The position of the follower is modeled as,

$$R_{k,l}^{4}(t+1)=M_{L,l}^{L}+\left(\cos\left(S_{k,l}(t)\right)*M_{L,l}^{L}*D_{k}(t)\right) \quad (12)$$

Let $M_{L,l}^{L}$ denote the position of the leader, L is the leading rider, $S_{k,l}(t)$ refers to the steering angle of the k^{th} rider in l^{th} coordinate at time t, $R_{k,l}^{4}(t+1)$ is the position of the follower, and $D_{k}(t)$ specifies the distance traveled by k^{th} rider at instant t. The distance $D_{k}(t)$ is computed using the velocity and off-time in which the velocity of k^{th} rider is calculated using the maximum speed, accelerator, gear, and brake with

respect to the vehicle of k^{th} rider. The selection of the co-ordinate selector depends on the on-time probability.

3.4.3 Position of overtaker

The overtaker updates the position using the direction indicator, coordinate selector, and success rate. The position of overtaker is given as,

$$R_{k,l}^{2}(t+1)=R_{k,l}(t)+\partial_{k}(t)*M_{L,l}^{L} \quad (13)$$

where, $R_{k,l}(t)$ is the position of k^{th} rider in l^{th} coordinate and $\partial_{k}(t)$ is the direction indicator corresponding to k^{th} rider at time t. The direction indicator $\partial_{k}(t)$ is given as,

$$\partial_{k}(t)=\left[\frac{2}{1-\log(SR)}\right]-1 \quad (14)$$

where, SR is the success rate of k^{th} rider at t and the success rate is computed using the multi-objective function. SR is computed based on the equation (21).

3.4.4 Position of attacker

The position update of the attacker is similar as the follower and the attacker updates the position using the following equation as,

$$R_{k,l}^{3}(t+1)=M_{L,l}^{L}+\left[\cos\left(S_{k,l}(t)\right)\right]*M_{L,l}^{L}+D_{k}(t) \quad (15)$$

3.5 Re-compute the Success Rate

The success rate of the riders is recomputed every-time after the rider groups update their positions to signify that the leader is not always the same rider.

3.6 Update the Parameters of the Rider

Once the success rate is re-evaluated, the optimization parameters, like the vehicles parameters of the rider, gear, steering angle, accelerator, brake, off-time, and activity counter are updated.

3.7 Termination

The steps are repeated until the destination is met by any of the rider groups, marking the announcement of the winner. Algorithm 1 shows the pseudocode of the proposed R-EHO algorithm.

Algorithm 1. R-EHO- Pseudo code

R-EHO algorithm	
1	Input : Rider's position $R_{k,l}(t)$
2	Output : Leading rider $M_{L,l}^{L}$
3	Start
4	Initialization
5	Rider population and riding parameters
6	Position angle $P_{k,l}(t)$
7	Steering angle $S_{k,l}(t)$
8	Accelerator A_k
9	Gear G_k
10	Coordinate angle $C_{k,l}(t)$
11	Brake B_k
12	Compute the success rate
13	While $t < t_{off}$
14	For $(k = 1 \ to \ N)$
	#Position update phase
15	eqn. (11) for updating the bypass riders' position
16	Followers' position using eqn. (12)
17	Overtakers' position using eqn. (13)
18	Follow eqn. (15) for attacker position update
19	Ranking the riders with respect to the success rate
20	Determine the leading rider
21	Update the Rider parameters
22	Return $M_{L,l}^{L}$
23	$t = t + 1$
24	End For
25	End While
26	Terminate

4. PROPOSED SPECTRAL UNMIXING USING THE R-EHO ALGORITHM BASED ON THE MULTIPLE OBJECTIVES

Spectral unmixing is a technique of extracting the valuable information from the hyperspectral image, which consists of the linear arrangement of the spectrum with the enormous proportion of the end members in individual pixels. In other words, the

scenes are captured using the spectral imaging technique and the captured spectra carries numerous signatures organized in spectra within a pixel. In general, any spectral unmixing technique involves three basic steps. In the first step, the estimation of the end members from the scene is progressed, followed with the identification of the spectral signatures. The third step is the computation of the fractional abundance from the individual end member belonging to the individual pixel. Most of the spectral unmixing methods in the literature follow the aforementioned steps. However, most of the methods suffer from the propagation errors, high computational cost, complexity issues, and poor accuracy in the first step of the end member estimation. Thus, there is a need for the effective estimation of the end member from the hyperspectral images for which the optimization is developed. The optimization named as, R-EHO is the integration of the EHO in ROA, which functions in estimating the end members and in computing the proportion of the signature. The computation of the fractional abundance follows the multi-objective function, which is designed based on the constraints, such as RSE, SPA, SNI, SNC, and mutual information. The spectral unmixing performed using the proposed optimization is found to be highly accurate and effective. Figure 1 shows the block diagram of the proposed method of spectral unmixing.

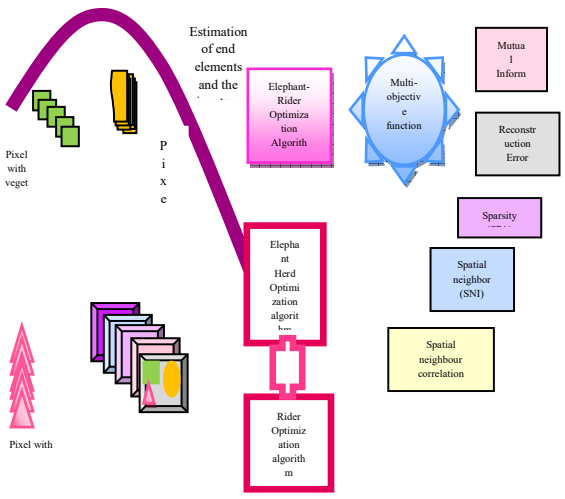

Figure 1. Spectral Unmixing Model Using The R-EHO Algorithm

4.1 Representation of the Hyperspectral Image

For spectral unmixing, the hyperspectral image is considered and the end members in the individual pixel of the image are performed. Let us denote the hyperspectral image I in the form of the matrix represented as,

$$I = \{h_1, \ldots, h_v\} \in J^{w \times v} \quad (16)$$

From the above equation, it is well understood that there are v number of the spectral vectors and w number of the spectral bands in a given input hyperspectral image. As per the Linear Mixture Model (LMM), the input image is rewritten as,

$$I = Y\,K + Q \text{ such that}$$
$$\mathrm{K} \geq 0 \;; 1_r^T K = 1_v^T \quad (17)$$

The input hyperspectral image is represented in terms of the mixing matrix and abundance matrix as in equation (17). The mixing matrix is given as,

$$Y = \left[y_1, \ldots, y_f, \ldots, y_r\right] \in J^{w \times v} \quad (18)$$

It is understood that there are r end members and the f^{th} signature corresponding to the end member as, y_f. Likewise, the abundance matrix is represented as, K and the abundance matrix is organized as,

$$K = \left[x_1, \ldots, x_f, \ldots, x_v\right] \in J^{w \times v} \quad (19)$$

The abundance matrix represents the fraction of the end members and x_f represents the f^{th} fraction corresponding to the end member such that f takes the value between 1 and v .The estimation of the end members is performed using the component, which assures the effective understanding regarding the abundance of the non-negativity constraint that is indicated as, $\mathrm{K} \geq 0$. Likewise, $1_r^T \mathrm{K} = 1_v^T$ represents the sum-to-one constraint that is computed through the physical interpretation belonging to the abundance vector and $1_r = [1, 1, \ldots, 1]^T$ is the column vector that acquires the dimension r. The term $[\,]^T$ represents the transposed vector elements. At the same time, the LMM representation of the input hyperspectral image carries an additional term Q, which represents the noise, affecting the

measurement. The estimation of the end members, which is the first step in spectral unmixing determines the r number of the end members using the abundance matrix K and mixing matrix Y. The basic idea behind the estimation of the end members is that from the total of r end members, the algorithm determines u end members and these estimated end members are confined in three conditions. The first condition is assumed to be the ideal condition in which the available end members and the estimated end members are equal. In the second condition, the estimated end members are less than the available end members in the hyperspectral image, which is represented as, $u<r$ and this condition is referred as the underestimated nature of the end members and this condition assist the analyst for the effective identification of a number of the end members from the image. The last condition represents the overestimation of the end member, represented as, $u>r$, and this condition is a sort of critical moment similar to that of the ideal condition, specifying the absence of any pure pixel in the captured image. This paper assumes the condition $u \geq r$ as r is unknown in advance and this condition specifies the overestimated state. Thus, the general idea is regarding the overestimation that enables the easy computation of the end members and this is not the real case in the presence of the exact number of the end members. The end members, mixing, and abundance matrices r, Y, and K are estimated using the R-EHO algorithm based on the multi-objective function.

4.2 Design the Objective Function based on Multiple Constraints

The end members and their abundance are estimated using the proposed R-EHO algorithm following the multi-objective function, which depends on four constraints, like RSE, SNC, SPA, SNI, and mutual information, respectively. The multi-objective function is given as in equation (5) for the existing spectral unmixing technique in [31].

$$\min_{U,V}\left\{\frac{1}{2}\|I-UV\|_F^b+\gamma\|V\|_{2,1}+\frac{\omega}{2}\|U-H\|_F^b\right\} \quad (20)$$

such that $V \in \chi_{u-1}$ $U \in W_{u-1}$

where, $\|\ \|_F$ and $\|\ \|_2$ is the Frobenius and Euclidean norms, respectively. $U \equiv [p_1,\ldots,p_u] \in \mathrm{P}^{u\times s}$ and $V \in J^{u\times v}$ are the optimization variables corresponding to the abundance and mixing matrices, respectively. The modified objective function is given as,

$$\min_{U,V}\left\{\frac{1}{2}\|I-UV\|_F^b+\gamma\|V\|_{2,1}+\frac{\omega}{2}\|U-H\|_F^b\right\}+\upsilon\left[\begin{array}{c}\left|\frac{1}{m*n*Z}\sum_{i=1}^{m}\sum_{j=1}^{n}(I-UV)-\sum_{\substack{s=1\\ s\in i,j}}^{8}(I-UV)_{i,j}^{s}\right|+\\ [\eta-MI(I,UV)]\end{array}\right] \quad (21)$$

The optimization, R-EHO estimates the end members along with their abundance using equation (21). The first term $\|I-U\ V\|_F^b$ highlights the data fidelity to enable minimal reconstruction errors, and the second term $\|V\|_{2,1}$ ensures the row sparsity for matrix V by fixing the complex rows to zero. The term, $\frac{\omega}{2}\|U-H\|_F^b$ pulls the columns in U to reach the solution H, which is the solution of the optimization, which along with matrix V drags the end members to reach the extreme. The term $\|V\|_{2,1}=\sum_{i=1}^{u}\|a\|_2$ specifies the SPA indicating the mixed norm of matrix V. The term, $\frac{\omega}{2}\|U-H\|_F^b$ is the SNI constraint and from this term, $H=\lfloor q_{i_1},\ldots,q_{i_u}\rfloor$ indicates u spectral vectors. γ and ω are the regularization parameters. χ_{u-1} represents the matrices with total dimension $(u\times v)$, where the columns specify the probability simplex with dimension $(u-1)$. W_{u-1} is the matrix of size $(w\times u)$, and the size of the columns are $(u-1)$, which highlights the data I. The term $\upsilon\left[\frac{1}{m*n*Z}\sum_{i=1}^{m}\sum_{j=1}^{n}(I-UV)-\sum_{\substack{s=1\\ s\in i,j}}^{8}(I-UV)_{i,j}^{s}\right]$ refers to the SNC parameter, which is calculated based on the average of the neighboring pixels. The constant, υ is the regularization parameter, m and n represent the rows and columns in $(I-U\ V)$. The objective function withstands the problems arising due to the violation of the sum-to-one constraints present in real data. The fifth term is, $[\eta-MI\ (I,U\ V)]$, which specifies the mutual information and the five constraints constitute the multi-objective function, which should be minimal

for the better solution, determined using the R-EHO algorithm.

5. RESULTS AND DISCUSSION

In this section, the results of the proposed spectral unmixing model based on the proposed R-EHO algorithm is deliberated with the elaborate description of the comparative methods and detailed discussion of various existing methods.

5.1 Experimental Setup

The experimentation is performed using the hyperspectral images and the implementation is done in MATLAB and the employed dataset is Urban and Cuprite data from [30]. The original image_1 is taken from urban dataset [30] and original image_2 is obtained from Cuprite data. The original image_1 possesses 307×307 pixels in $[2 \times 2]$ m^2 area and the wavelength range of the image is 210 wavelengths between 400 nm and 2500 nm and holds the spectral resolution of 10 nm. There are three ground truths for the urban data along with 4, 5 and 6 end members respectively and the end members include Asphalt, Roof, Grass, Tree, Metal, and Dirt. The cuprite data possesses 224 channels of the range between 370 nm and 2480 nm. The region consists of 250 x 190 pixels with a total of 14 mineral types. There are meagre differences in the variants of similar minerals, and a total of 12 end members are used that includes Alunite, Andradite, Pyrope, Buddingtonite, Kaolinite1, Dumortierite, Sphene, Muscovite, Kaolinite2, Nontronite, Montmorillonite, and Chalcedony.

5.2 Experimental Analysis

In this section, the experimental analysis of the methods is presented with the images taken from the databases, Urban and cuprite dataset. Figure 2 depicts the original images and corresponding reflectances taken from the urban dataset. Figure 2 i) shows the original image_1 and figure 2 ii) is the reflectance graph corresponding to the original image_1. Figure 2 iii) shows the original image_2 and figure 2 iv) is the reflectance graph corresponding to the original image_2.

i)

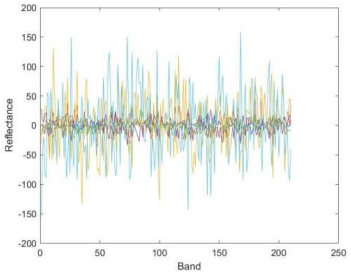

ii)

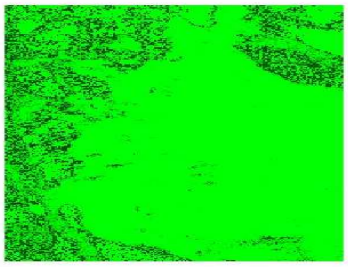

iii)

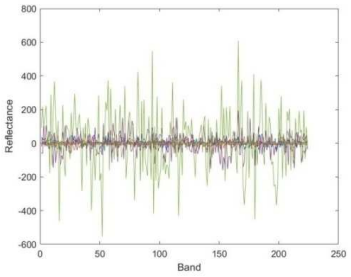

iv)

Figure 2. *Original Images, I) Original Image_1, Ii) Reflectance Graph Of Original Image_1, Iii) Original Image_2, Iv) Reflectance Graph Of Original Image_2*

Figure 3 shows the end members corresponding to the original image_1 and the end members are deliberated in figure 3 i), figure 3 ii), figure 3 iii), figure 3 iv), figure 3 v), and figure 3 vi), respectively.

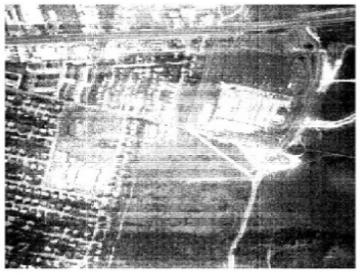

i)

ii)

iii)

iv)

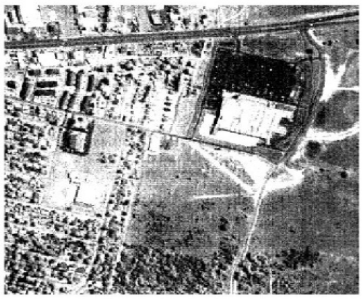

v)

vi)

Figure 3. *Original End Members Of Original Image_1, I) End Member_1, Ii) End Member_2, Iii) End Member_3, Iv) End Member_4, V) End Member_5, Vi) End Member_6*

Figure 4 shows the estimated end members from the original image_1 using the proposed R-EHO algorithm. The estimated end members from the original image_1 is depicted in figure 4 i), figure 4 ii), figure 4 iii), figure 4 iv), figure 4 v), and figure 4 vi), respectively.

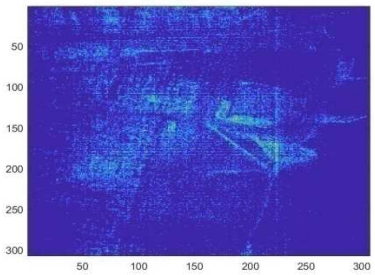

i)

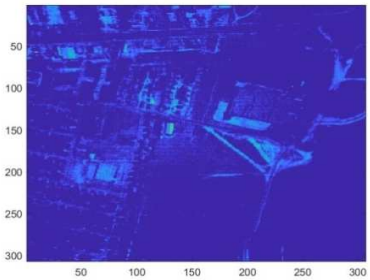

ii)

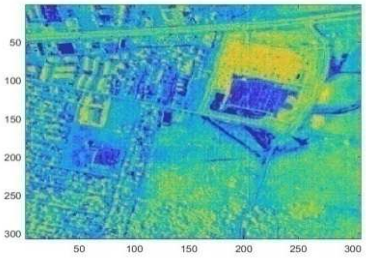

iii)

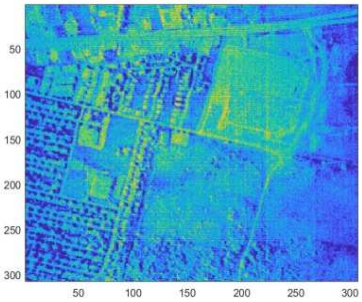

iv)

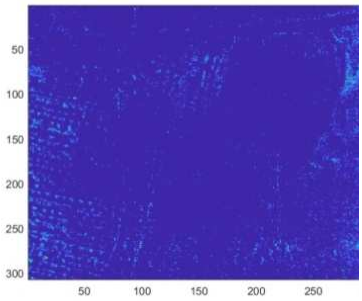

v)

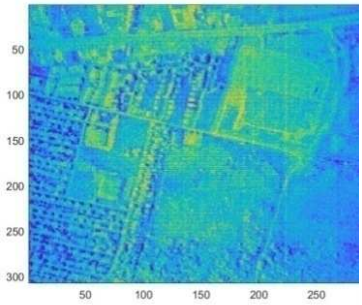

vi)

Figure 4. Estimated End Members Of Original Image_1 Using R-EHO-Based Spectral Unmixing, I) Estimated End Member_1, Ii) Estimated End Member_2, Iii) Estimated End Member_3, Iv) Estimated End Member_4, V) Estimated End Member_5, Vi) Estimated End Member_6

Figure 5 shows the original end members corresponding to the original image_2 and the end members are deliberated in figure 5 i), figure 5 ii), figure 5 iii), figure 5 iv), figure 5 v), figure 5 vi), figure 5 vii), figure 5 viii), figure 5 ix), figure 5 x), figure 5 xi), and figure 5 xii), respectively.

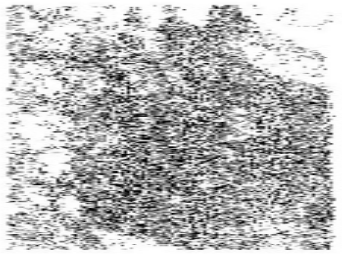

i)

ii)

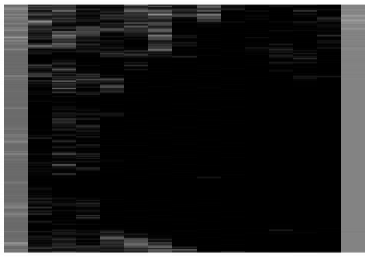

iii)

iv)

v)

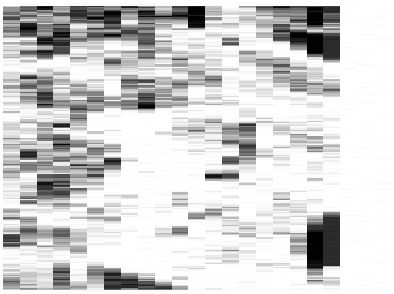

vi)

vii)

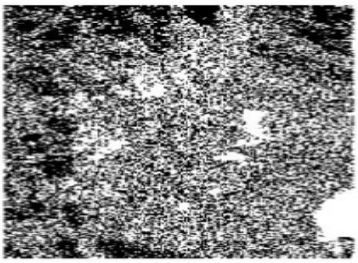

viii)

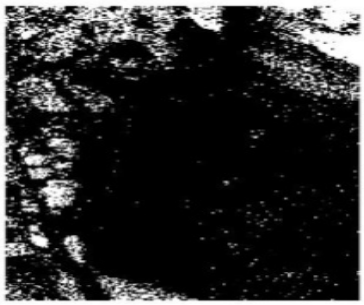

ix)

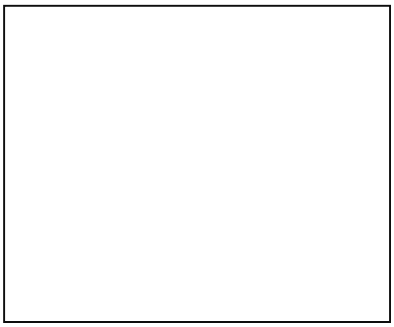

x)

xi)

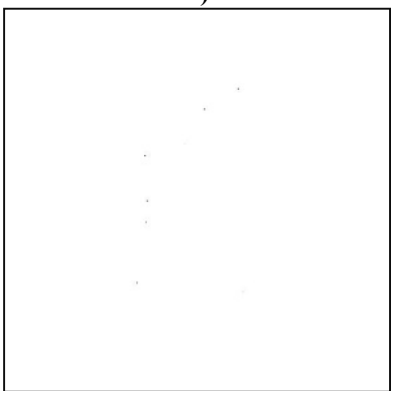

xii)

Figure 5. Original End Members Of Original Image_2, I) End Member_1, Ii) End Member_2, Iii) End Member_3, Iv) End Member_4, V) End Member_5, Vi) End Member_6, Vii) End Member_7, Viii) End Member_8, Ix) End Member_9, X) End Member_10, Xi) End Member_11, Xii) End Member_12

Figure 6 shows the estimated end members corresponding to the original image_2 and the end members are deliberated in figure 6 i), figure 6 ii), figure 6 iii), figure 6 iv), figure 6 v), figure 6 vi), figure 6 vii), figure 6 viii), figure 6 ix), figure 6 x), figure 6 xi), and figure 6 xii), respectively.

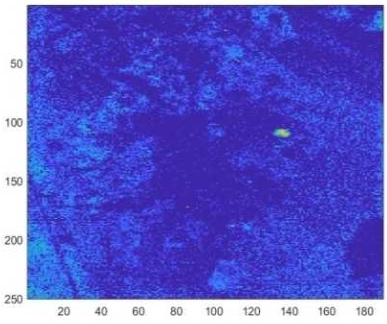

i)

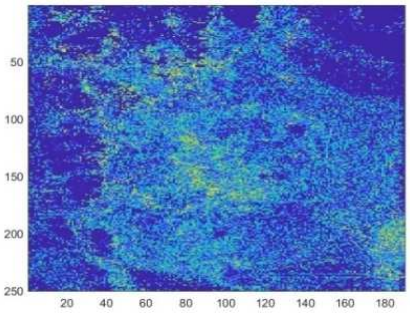

ii)

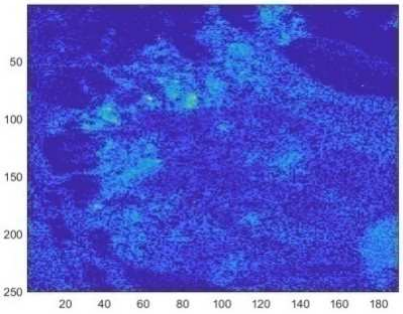

iii)

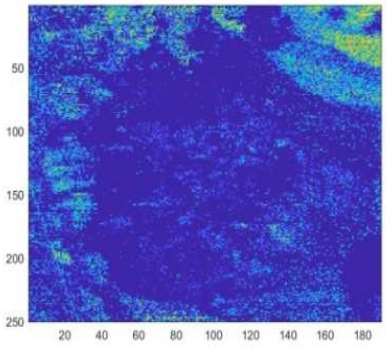

iv)

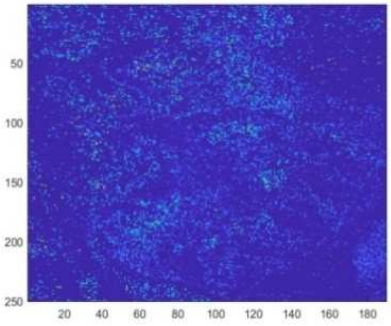

v)

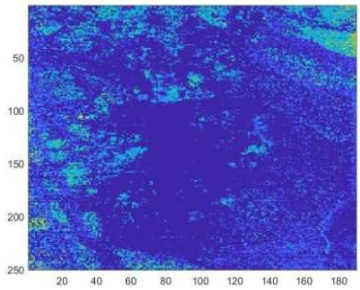

vi)

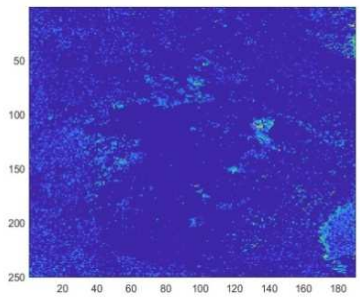

vii)

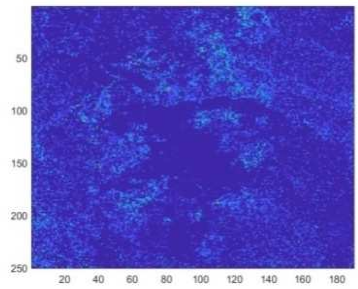

viii)

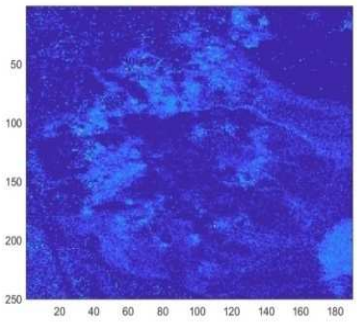

ix)

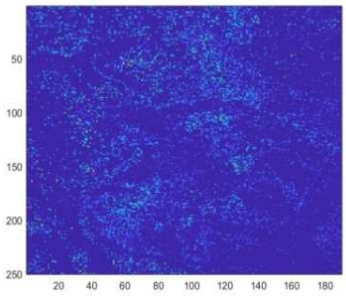

x)

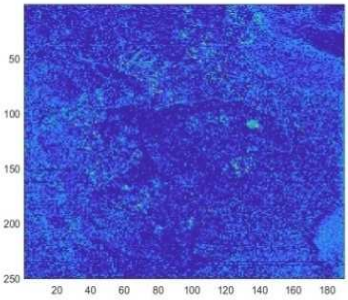

xi)

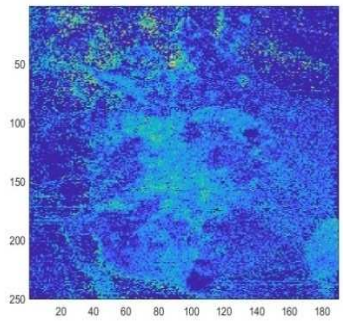

xii)

Figure 6. Estimated End Members Of Original Image_2, I) Estimated End Member_1, Ii) Estimated End Member_2, Iii) Estimated End Member_3, Iv) Estimated End Member_4, V) Estimated End Member_5, Vi) Estimated End Member_6, Vii) Estimated End Member_7, Viii) Estimated End Member_8, Ix) Estimated End Member_9, X) Estimated End Member_10, Xi) Estimated End Member_11, Xii) Estimated End Member_12

5.3 Performance Metrics

The performance evaluation of the proposed SU is done based on two metrics, such as RMSE and RE that enable the effective comparison of the proposed method with the existing method. The metrics are formulated as follows:

5.3.1 RMSE

The RMSE of the methods is given as,

$$RMSE_f = \sqrt{\frac{1}{v}\sum_{j=1}^{v}\left(x_{fj} - \hat{x}_{fj}\right)^2} \quad (22)$$

where, v is the total pixel, x_{fj} refers to the real abundance fraction for f^{th} end member in j^{th} pixel, and $\hat{x}_{fj}$ refers to the estimated end members. Thus,

$$RMSE = \sum_{f=1}^{r} RMSE_f \quad (23)$$

where, r symbolizes the extracted end members and $RMSE_f$ corresponds to the RMSE of the individual pixels. Any effective method reports with the minimal value of RMSE to symbolize the effective performance.

5.3.2 RE

The RE of the methods is computed as,

$$RE = x - \hat{x}_{ff}^2 \quad (24)$$

where, x refers to the true abundance matrix and $\hat{x}$ indicates the estimated abundance matrix. The accurate estimation is indicated by the smaller value of RE.

5.3.4 Reflectance of the end member

The reflectance of a pixel is computed as per the equation (17), which is calculated using the reflectance of individual end member in a band, fractional abundance, and errors in the band.

5.4 Performance Analysis

The performance analysis of the methods is deliberated in this section and the analysis is

performed using two original images. Figure 7 shows the performance analysis using the original image_1. Figure 7 i) shows the analysis based on RE of the methods. The RE of the R-EHO method based on the population size 5, 10, 15, 20, and 25 is 61.2490, 51.4851, 42.7426, 34.7466, 17.1446, and 10.4680, respectively. Figure 7 ii) shows the analysis based on RMSE of the methods. The RMSE of the R-EHO method based on the population size 5, 10, 15, 20, and 25 is 0.0814, 0.0617 , 0.0462, 0.0412, 0.0139, and 0.0011, respectively.

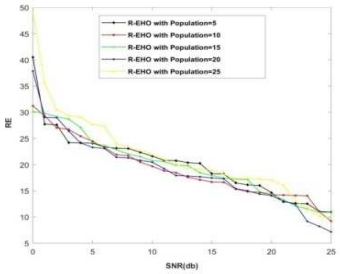

i)

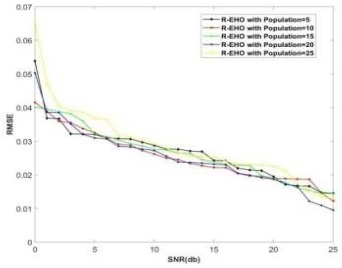

ii)

Figure 7. Performance Analysis Using Original Image_1, I) Performance Analysis Based On RE, Ii) Performance Analysis Based On RMSE

Figure 8 shows the analysis using the end members through analyzing the reflectance with respect to the band. Figure 8 i) shows the analysis using estimated end member_1 of original image_1. The reflectance of end member_1 at band 50 is 0.1098 %, -0.5706 %, -0.0287 %, -0.0454 %, -0.1493 %, and 0.1473 %, respectively. Figure 8 ii) shows the analysis using estimated end member_2 of original image_1. The reflectance of end member_2 at band 50 is 0.1555 %, 0.0458 %, -0.2503 %, -0.0004 %, -0.0288 %, and 0.0441 %, respectively. Figure 8 iii) shows the analysis using estimated end member_3 of original image_1. The reflectance of end member_3 at band 50 is 0.0479 %, 0.4535 %, -0.0757 %, -0.0216 %, -0.0165 %, and 0.0639 %, respectively.

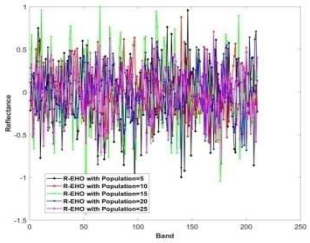

i)

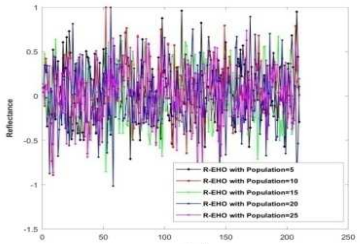

ii)

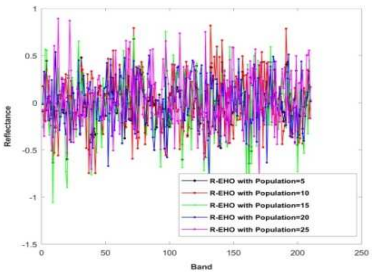

iii)

Figure 8. Performance Analysis Using The Estimated End Members Of Original Image_1, I) Performance Analysis Using End Member_1, Ii) Performance Analysis Using End Member_2, Iii) Performance Analysis Using End Member_3

Figure 9 shows the analysis using the end members through analyzing the reflectance with respect to the band. Figure 9 i) show the analysis using estimated end member_4 of original image_1. The reflectance of end member_4 at band 50 is 0.0538 %, 0.2803 %, -0.3188 %, 0.0548 %, 0.0291 %, and 0.2325 %, respectively. Figure 9 ii) shows the analysis using estimated end member_5 of original image_1. The reflectance of end member_5 at band 50 is 0.5264 %, -0.0045 %, -0.2466 %, -0.0983 %, 0.0670 %, and -0.0149 %, respectively. Figure 9 iii) shows the analysis using estimated end member_6 of original image_1. The reflectance of end member_6 at band 50 is 0.0233 %, 0.0342 %, -

0.2950 %, -0.0006 %, -0.4060 %, and 0.0550 %, respectively.

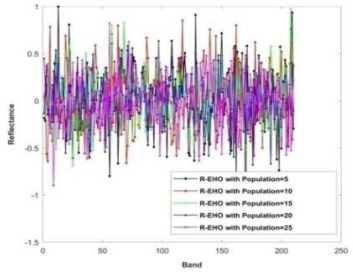

i)

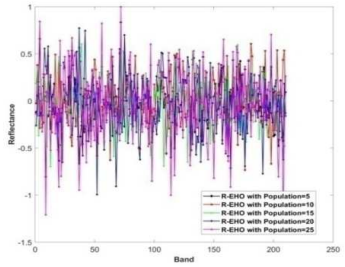

ii)

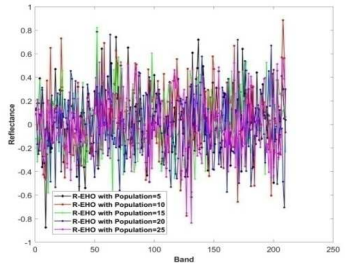

iii)

Figure 9. Performance Analysis Using The Estimated End Members Of Original Image_1, I) Performance Analysis Using End Member_4, Ii) Performance Analysis Using End Member_5, Iii) Performance Analysis Using End Member_6

Figure 10 shows the performance analysis using the original image_2. Figure 10 i) shows the analysis based on RE of the methods. The RE of the R-EHO method based on the population size 5, 10, 15, 20, and 25 is 12.8489, 15.9104, 12.9897, 12.4654, and 15.9371, respectively. Figure 10 ii) shows the analysis based on RMSE of the methods. The RMSE of the R-EHO method based on the population size 5, 10, 15, 20, and 25 is 0.0170, 0.0211, 0.0172, 0.0165, and 0.0211, respectively.

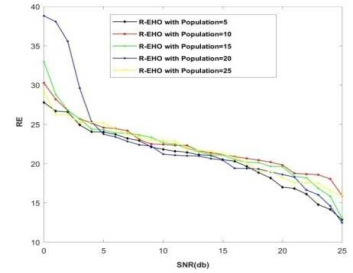

i)

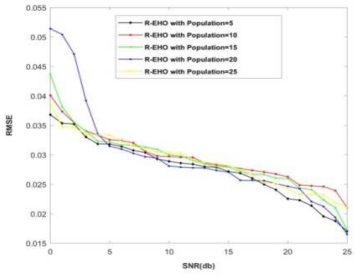

ii)

Figure 10. Performance Analysis Using Original Image_2, I) Performance Analysis Based On RE, Ii) Performance Analysis Based On RMSE

Figure 11 shows the analysis using the end members through analyzing the reflectance with respect to the band. Figure 11 i) show the analysis using estimated end member_1 of original image_2. The reflectance of end member_1 at band 50 is -0.2004 %, 0.3867 %, -0.4072 %, 0.0932 %, -0.2075 %, and 0.0166 %, respectively. Figure 11 ii) shows the analysis using estimated end member_2 of original image_2. The reflectance of end member_2 at band 50 is 0.2835 %, -0.0335 %, -0.1558 %, 0.0519 %, 0.2777 %, and 0.0448 %, respectively. Figure 11 iii) shows the analysis using estimated end member_3 of original image_2. The reflectance of end member_3 at band 50 is -0.5053 %, -0.4861 %, 0.1484 %, -0.3545 %, -0.1460 %, and 0.1294 %, respectively. Figure 11 iv) shows the analysis using estimated end member_4 of original image_2. The reflectance of end member_4 at band 50 is -0.0079 %, 0.5408 %, 0.3933 %, 0.1099 %, 0.4387 %, and -0.1235 %, respectively.

Journal of Theoretical and Applied Information Technology
15th April 2022. Vol.100. No 7

ISSN: 1992-8645 www.jatit.org E-ISSN: 1817-3195

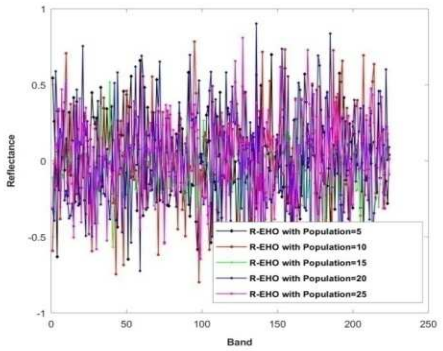

i)

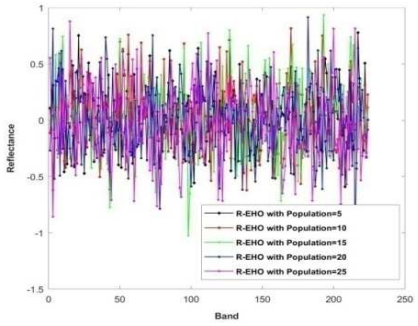

ii)

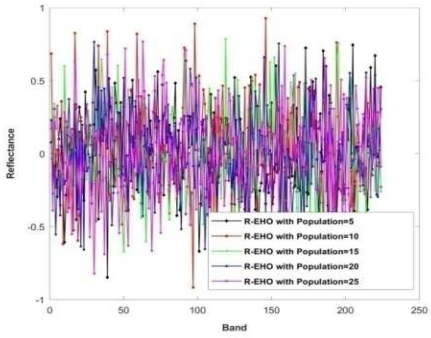

iii)

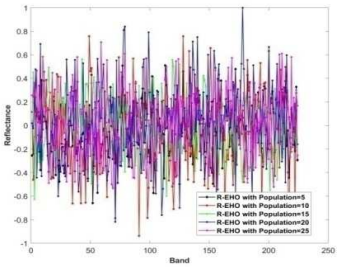

iv)

Figure 11. Performance Analysis Using The Estimated End Members Of Original Image_2, I) Performance Analysis Using End Member_1, Ii) Performance Analysis Using End Member_2, Iii) Performance Analysis Using End Member_3, Iv) Performance Analysis Using End Member_4

Figure 12 shows the analysis using the end members through analyzing the reflectance with respect to the band. Figure 12 i) show the analysis using estimated end member_5 of original image_2. The reflectance of end member_5 at band 50 is 0.2027 %, 0.0927 %,-0.3791 %, -0.1766 %, 0.0598 %, and 0.2915 %, respectively. Figure 12 ii) shows the analysis using estimated end member_6 of original image_2. The reflectance of end member_6 at band 50 is 0.2854 %, 0.3095 %, -0.0471 %, -0.0092%, -0.3053 %, and -0.1690 %, respectively. Figure 12 iii) shows the analysis using estimated end member_7 of original image_2. The reflectance of end member_7 at band 50 is 0.3251 %, -0.0524 %, -0.1347 %, 0.0293 %, 0.0101 %, and 0.1789 %, respectively. Figure 12 iv) shows the analysis using estimated end member_8 of original image_2. The reflectance of end member_8 at band 50 is 0.4431 %, -0.0881 %, 0.4866 %, 0.0063 %, -0.7057 %, and -0.0076 %, respectively.

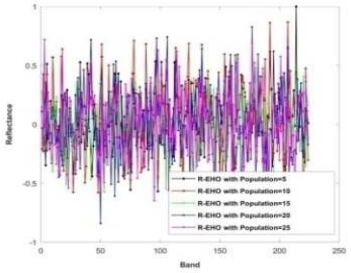

i)

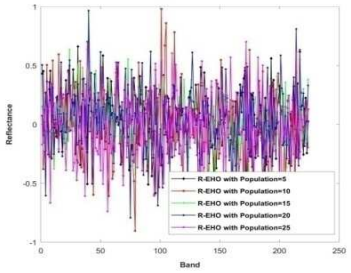

ii)

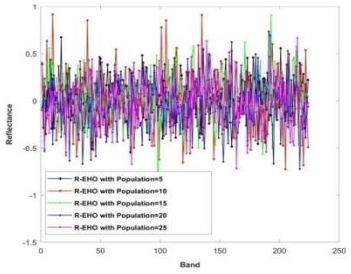

iii)

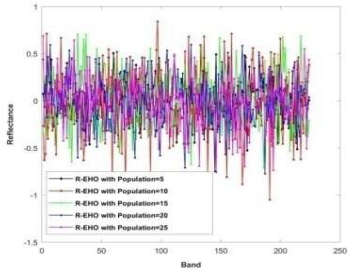

iv)

Figure 12. Performance Analysis Using The Estimated End Members Of Original Image_2, I) Performance Analysis Using End Member_5, Ii) Performance Analysis Using End Member_6, Iii) Performance Analysis Using End Member_7, Iv) Performance Analysis Using End Member_8

Figure 13 shows the analysis using the end members through analyzing the reflectance with respect to the band. Figure 13 i) show the analysis using estimated end member_9 of original image_2. The reflectance of end member_9 at band 50 is 0.4327 %, -0.0805 %, 0.1255 %, -0.0070 %, 0.6747 %, and -0.0417 %, respectively. Figure 13 ii) shows the analysis using estimated end member_10 of original image_2. The reflectance of end member_10 at band 50 is 0.1037 %, 0.0559 %, 0.0371 %, 0.0480 %, -0.5489 %, and 0.2083 %, respectively. Figure 13 iii) shows the analysis using estimated end member_11 of original image_2. The reflectance of end member_11 at band 50 is -0.0735 %, -0.2017 %, 0.1427 %, -0.3773 %, 0.5749 %, and -0.0133 %, respectively. Figure 13 iv) shows the analysis using estimated end member_12 of original image_2. The reflectance of end member_12 at band 50 is -0.0532 %, 0.4638 %,-0.2102 %, 0.4089 %, 0.4360 %, and 0.0696 %, respectively.

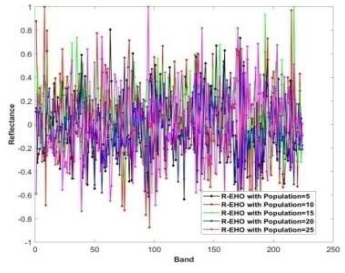

i)

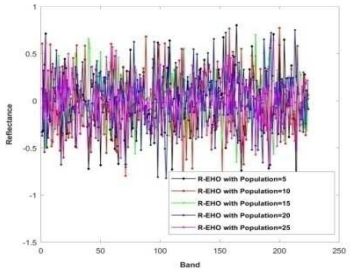

iii)

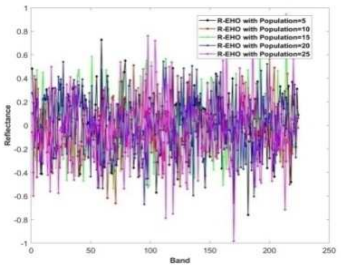

iii)

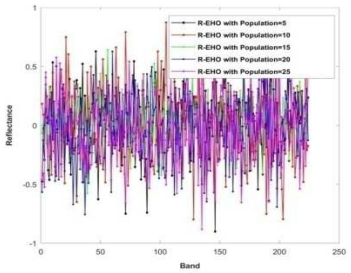

iv)

Figure 13. Performance Analysis Using The Estimated End Members Of Original Image_2, I) Performance Analysis Using End Member_9, Ii) Performance Analysis Using End Member_10, Iii) Performance Analysis Using End Member_11, Iv) Performance Analysis Using End Member_12

5.5 Competing Methods

The methods employed for comparing the proposed spectral unmixing includes: bi-objective optimization model (Bi-MOSU) and tri-objective optimization model (Tri-MOSU) [2], Pareto multi-objective based sparse unmixing (Pareto- MOSU) [32], Robust collaborative Non-negative matrix Factorization (R-CoNMF) [26], and Rider Optimization Algorithm (ROA) [11]. Additionally, Lion Rider Optimization (LRO) is employed as the comparative method for the spectral unmixing and LRO is the integration of the Lion Optimization (LOA) in Rider Optimization algorithm (ROA).

5.6 Comparative Analysis

This section presents the comparative analysis of the methods based on the end members estimated and based on the performance metrics. The analysis is performed using two images, original image_1 and original image_2.

5.6.1 Comparative analysis based on the original image_1 depending on the performance metrics

The comparison of the methods based on the performance metrics, RE and RMSE are performed in this section using the original image_1. Figure 14 shows the comparative analysis based on RE and RMSE and figure 14 i) shows the comparative analysis based on RE. The RE of the methods, Bi-MOSU + Tri-MOSU, R-CoNMF, Pareto-MOSU, ROA, LRO, and proposed R-EHO is 61.2490, 51.4851, 42.7426, 34.7466, 17.1446, and 10.4680, when the SND is 25dB. Figure 14 ii) shows the comparative analysis based on RMSE. The RMSE of the methods, Bi-MOSU + Tri-MOSU, R-CoNMF, Pareto-MOSU, ROA, LRO, and proposed R-EHO is 0.0814, 0.0617, 0.0462, 0.0412, 0.0139, and 0.0011, when the SND is 25dB. It is clear that the proposed R-EHO method acquires the minimal RMSE and minimal RE when compared with the existing methods.

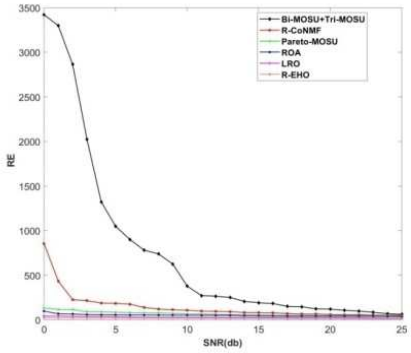

i)

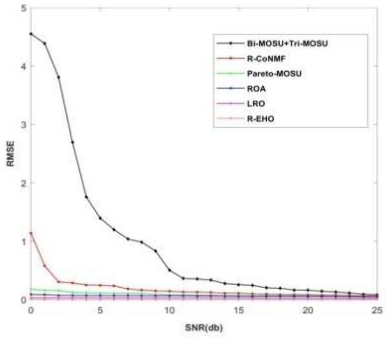

ii)

Figure 14. Comparative Analysis Using Original Image_1, I) Performance Analysis Based On RE, Ii) Performance Analysis Based On RMSE

5.6.2 Comparative analysis using the end members of original image_1

Figure 15 shows the comparative analysis using the end members of the original image_1. Figure 15 i) show the comparative analysis using the end member_1. The reflectance of the methods, Bi-MOSU + Tri-MOSU, R-CoNMF, Pareto-MOSU, ROA, LRO, and proposed R-EHO is 0.2388 %, -0.3399 %, 0.1744 %, 0.4246 %, and -0.2585 %, respectively for band 50. Figure 15 ii) show the comparative analysis using the end member_2. The reflectance of the methods, Bi-MOSU + Tri-MOSU, R-CoNMF, Pareto-MOSU, ROA, LRO, and proposed R-EHO is 0.5260 %, 0.0664 %, 0.1850 %, 0.2539 %, and -0.2303 %, respectively for band 50. Figure 15 iii) show the comparative analysis using the end member_3. The reflectance of the methods, Bi-MOSU + Tri-MOSU, R-CoNMF, Pareto-MOSU, ROA, LRO, and proposed R-EHO is -0.1373 %, 0.0759 %, -0.0591 %, 0.1672 %, and -0.0857 %, respectively for band 50.

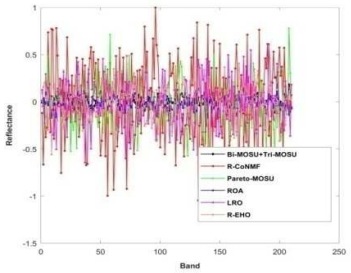

i)

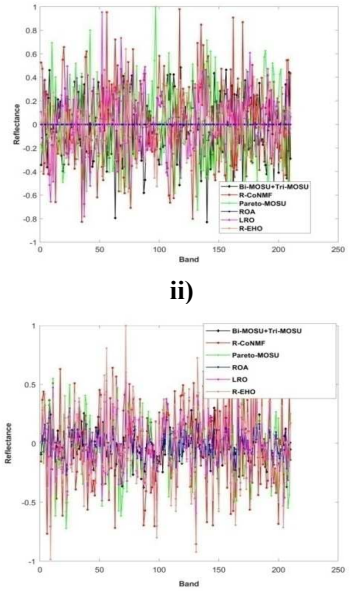

ii)

iii)

Figure 15. Comparative Analysis Using The End Members Of Image_1, I) End Member_1, Ii) End Member_2, Iii) End Member_3

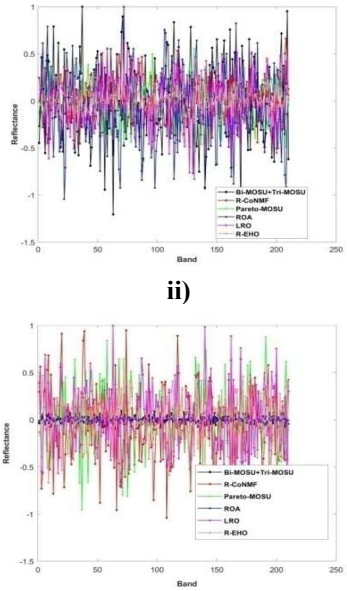

ii)

iii)

Figure 16. Comparative Analysis Using The End Members Of Image_1, I) End Member_4, Ii) End Member_5, Iii) End Member_6

Figure 16 shows the comparative analysis using the end members of the original image_1. Figure 16 i) show the comparative analysis using the end member_4. The reflectance of the methods, Bi-MOSU + Tri-MOSU, R-CoNMF, Pareto-MOSU, ROA, LRO, and proposed R-EHO is 0.0942%, -0.2619 %, 0.0626 %, 0.1741 %, and -0.0768 %, respectively for band 50. Figure 16 ii) show the comparative analysis using the end member_5. The reflectance of the methods, Bi-MOSU + Tri-MOSU, R-CoNMF, Pareto-MOSU, ROA, LRO, and proposed R-EHO is 0.1924 %, 0.4386 %, 0.062 %, -0.01 %, and -0.4193 %, respectively for band 50. Figure 16 iii) show the comparative analysis using the end member_6. The reflectance of the methods, Bi-MOSU + Tri-MOSU, R-CoNMF, Pareto-MOSU, ROA, LRO, and proposed R-EHO is 0.2819%, 0.0886 %, 0.1131 %, - 0.4480 %, and 0.0962 %, respectively for band 50.

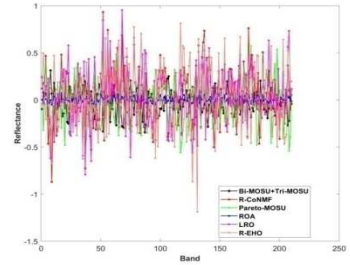

i)

5.6.2 Comparative analysis based on the original image_2 depending on the performance metrics

The comparison of the methods based on the performance metrics, RE and RMSE are performed in this section using the original image_2. Figure 17 shows the comparative analysis based on RE and RMSE and figure 17 i) shows the comparative analysis based on RE. The RE of the methods, Bi-MOSU + Tri-MOSU, R-CoNMF, Pareto-MOSU, ROA, LRO, and proposed R-EHO is 94.7656, 82.5873, 60.9128, 43.4902, 19.2401, and 13.8576, when the SNR is 25dB. Figure 17 ii) shows the comparative analysis based on RMSE. The RMSE of the methods, Bi-MOSU + Tri-MOSU, R-CoNMF, Pareto-MOSU, ROA, LRO, and proposed R-EHO is 0.1255, 0.0807, 0.0576, 0.0533, 0.0184, and 0.0048, when the SND is 25dB. It is clear that the proposed R-EHO method acquires the minimal RMSE and minimal RE when compared with the existing methods.

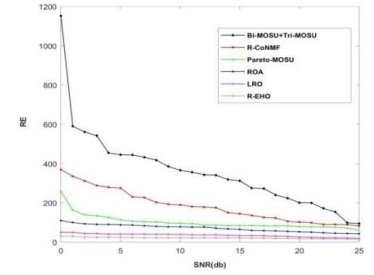

i)

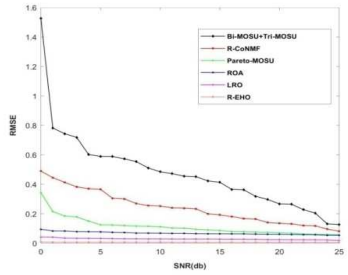

6

ii)

Figure 17. Comparative Analysis Using Original Image_2, I) Performance Analysis Based On RE, Ii) Performance Analysis Based On RMSE

Figure 18 shows the comparative analysis using the end members of the original image_2. Figure 18 i) show the comparative analysis using the end member_1. The reflectance of the methods using end member_1, Bi-MOSU + Tri-MOSU, R-CoNMF, Pareto-MOSU, ROA, LRO, and proposed R-EHO is 0.4360 %, 0.4616 %, 0.037 %, -0.0789 %, and 0.3112 %, respectively for band 50. Figure 18 ii) show the comparative analysis using the end member_2. The reflectance of the methods using end member_2, Bi-MOSU + Tri-MOSU, R-CoNMF, Pareto-MOSU, ROA, LRO, and proposed R-EHO is 0.1911 %, 0.6977 %, 0.7234 %, -0.0631 %, and 0.2376 %, respectively for band 50. Figure 18 iii) show the comparative analysis using the end member_3. The reflectance using end member_3 of the methods, Bi-MOSU + Tri-MOSU, R-CoNMF, Pareto-MOSU, ROA, LRO, and proposed R-EHO is 0.3199%, -0.2201 %, -0.6707 %, 0.5184 %, and -0.2885 %, respectively for band 50. Figure 18 iv) show the comparative analysis using the end member_4. The reflectance using end member_4 of the methods, Bi-MOSU + Tri-MOSU, R-CoNMF, Pareto-MOSU, ROA, LRO, and proposed R-EHO is -0.1573%, 0.4602 %, 0.0451 %, - 0.0704 %, and 0.2605 %, respectively for band 50.

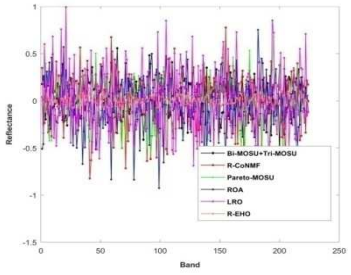

i)

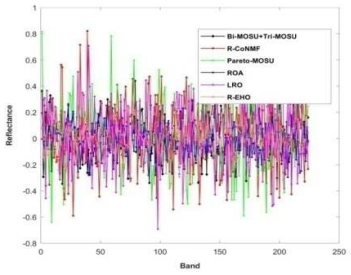

ii)

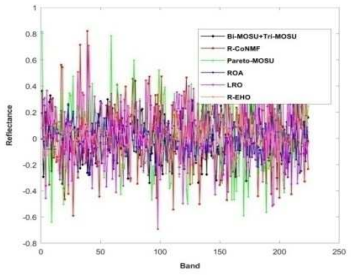

iii)

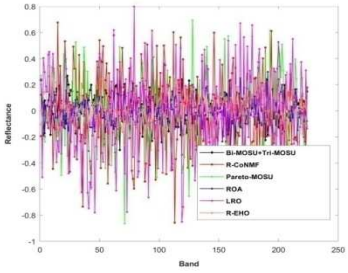

iv)

Figure 18. Comparative Analysis Using The End Members Of Image_2, I) End Member_1, Ii) End Member_2, Iii) End Member_3, Iv) End Member_4

Figure 19 shows the comparative analysis using the end members of the original image_2. Figure 19 i) show the comparative analysis using the end member_5. The reflectance of the methods using end member_5, Bi-MOSU + Tri-MOSU, R-CoNMF, Pareto-MOSU, ROA, LRO, and proposed R-EHO is 0.3450 %, -0.2604 %, 0.3724 %, -0.8402 %, and -0.5649 %, respectively for band 50. Figure

19 ii) show the comparative analysis using the end member_6. The reflectance of the methods using end member_6, Bi-MOSU + Tri-MOSU, R-CoNMF, Pareto-MOSU, ROA, LRO, and proposed R-EHO is -0.1267 %, -0.1198 %, 0.1413 %, 0.6138 %, and -0.3907 %, respectively for band 50. Figure 19 iii) show the comparative analysis using the end member_7. The reflectance using end member_7 of the methods, Bi-MOSU + Tri-MOSU, R-CoNMF, Pareto-MOSU, ROA, LRO, and proposed R-EHO is 0.4503 %, -0.3869 %, 0.3632 %, 0.3083 %, and -0.3617 %, respectively for band 50. Figure 19 iv) show the comparative analysis using the end member_8. The reflectance using end member_8 of the methods, Bi-MOSU + Tri-MOSU, R-CoNMF, Pareto-MOSU, ROA, LRO, and proposed R-EHO is 0.2213 %, -0.1797 %, -0.2257 %, 0.2171 %, and 0.2218 %, respectively for band 50.

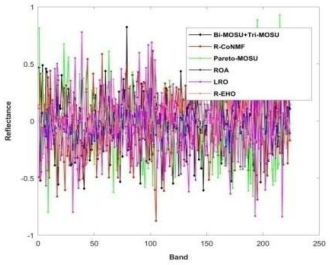

i)

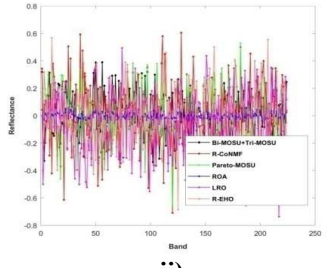

ii)

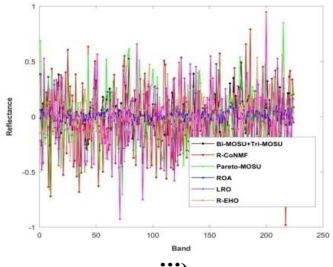

iii)

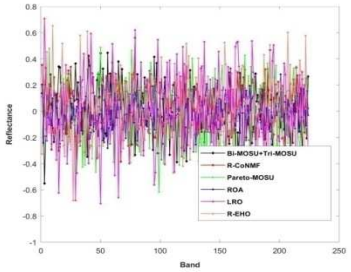

iv)

Figure 19. Comparative Analysis Using The End Members Of Image_2, I) End Member_5, Ii) End Member_6, Iii) End Member_7, Iv) End Member_8

Figure 20 shows the comparative analysis using the end members of the original image_2. Figure 20 i) show the comparative analysis using the end member_9. The reflectance of the methods using end member_9, Bi-MOSU + Tri-MOSU, R-CoNMF, Pareto-MOSU, ROA, LRO, and proposed R-EHO is -0.5441 %, -0.0731 %, 0.1184 %, -0.5136 %, and 0.5269 %, respectively for band 50. Figure 20 ii) show the comparative analysis using the end member_10. The reflectance of the methods using end member_10, Bi-MOSU + Tri-MOSU, R-CoNMF, Pareto-MOSU, ROA, LRO, and proposed R-EHO is -0.6823%, 0.1039 %, 0.5173 %, 0.3126 %, and -0.3622 %, respectively for band 50. Figure 20 iii) show the comparative analysis using the end member_11. The reflectance using end member_11 of the methods, Bi-MOSU + Tri-MOSU, R-CoNMF, Pareto-MOSU, ROA, LRO, and proposed R-EHO is 0.0089 %, -0.1676 %, -0.0004 %, -0.4341 %, and 0.0213 %, respectively for band 50. Figure 20 iv) show the comparative analysis using the end member_12. The reflectance using end member_12 of the methods, Bi-MOSU + Tri-MOSU, R-CoNMF, Pareto-MOSU, ROA, LRO, and proposed R-EHO is 0.0958 %, -0.3257 %, 0.4400 %, -0.0034 %, and 0.3088 %, respectively for band 50.

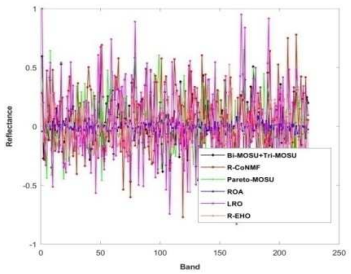

i)

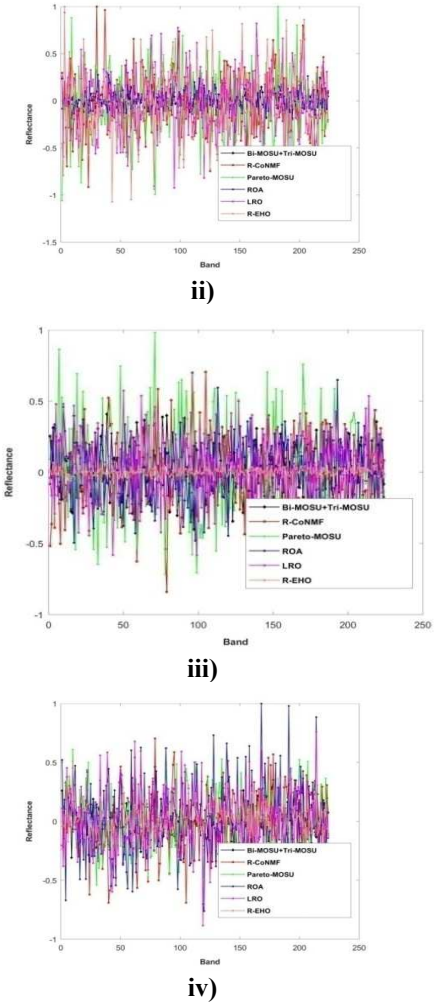

Figure 20. Comparative Analysis Using The End Members Of Image_2, I) End Member_9, Ii) End Member_10, Iii) End Member_11, Iv) End Member_12

5.9 Comparative Discussion

The research contribution of R-EHO is determined by the estimation of endmembers from each mixed pixel. The sparse based spectral unmixing approach using R-EHO multi-objective optimization technique achieves the global convergence by simultaneously optimizing the objective functions terms namely sparsity, spatial neighbour, spatial neighbour correlation, mutual information and reconstruction error.

The comparative discussion shows the effectiveness of the proposed R-EHO algorithm in spectral unmixing and table 1 shows the numerical justification of the methods. It is clear from the table 1 that the proposed R-EHO spectral unmixing outperformed the existing methods with a minimal RMSE and minimal RE of 0.0011 and 13.8576, respectively.

Table 1. Comparative Discussion

Methods	Bi-MOSU + Tri-MOSU	R-CoNMF	Pareto-MOSU	ROA	LRO	**Proposed R-EHO**
RMSE	0.037005	0.03865	0.03525	0.0317	0.0297	0.0011
RE	27.9002	26.5546	29.1082	23.8836	22.4027	13.8576

5.10 Difference from the prior research

The R-EHO is the hybrid computational approach of incorporating the Rider Optimization Algorithm (ROA) in the Elephant Herd Optimization method. The ROA method is developed on a fictious computer paradigm, not like other artificial computing algorithms and nature inspired algorithms that are based on real world data.

6. CONCLUSION

The paper demonstrates the spectral unmixing model based on a hybrid optimization, Rider-Elephant Herd Optimization (R-EHO) algorithm. The fractional abundances in the end members are estimated using the proposed optimization algorithm through the application of the multi-objective function, which is designed using the RSE, SPA, SNI, SNC, and mutual information. The R-EHO algorithm is the integration of the standard EHO in the existing ROA in such a way that the characteristics of the standard ROA is enhanced with the characteristics of EHO so that the convergence speed and the global optimal convergence is enhanced. The analysis of the methods is performed using the Cuprite and Urban dataset, which possesses 6 and 12 end members, respectively. The analysis is progressed using the end members and the comparative discussion is done with respect to the performance metrics, RMSE and RE. The proposed R-EHO algorithm for spectral unmixing reported with the minimal RMSE and minimal RE of 0.0011 and 13.8576, respectively. In the future, this research work would extend the research opportunities in evolutionary computing to incorporate multiple objectives pertaining to the bio-inspired or nature inspired computing so that the optimum solutions could be attained for the computationally complex problems which high dimensional data sources. The proposed R-EHO would be compatible with linear spectral unmixing paradigm which would compromise in extreme high dimensional dataset

manipulations and could be controlled by enhancing the algorithm as a non-linear computing model for enhanced versions of endmemers estimations. The R-EHO spectral unmixing algorithm will be improved by looking into possible nature-inspired computational models for long-term fractional abundance estimation and end member quantification in deep CNN architecture.

REFERENCES

[1] Shaoquan Zhang, Jun Li, Zebin Wu and Antonio Plaza, "Spatial Discontinuity-Weighted Sparse Unmixing of Hyperspectral Images," IEEE Trans. Geoscience and Remote Sensing, Vol. 56 , no. 10, pp. 5767 - 5779 , Oct. 2018.

[2] Xiangming Jiang, Maoguo Gong and Jun Li," A Two-Phase Multiobjective Sparse Unmixing Approach for Hyperspectral Data," IEEE Transactions on Geoscience and Remote Sensing ,Vol. 56 , no: 1, pp. 508 - 523, Jan. 2018.

[3] Dan Wang , Zhenwei Shi , and Xinrui Cui, "Robust Sparse Unmixing for Hyperspectral Imagery," IEEE Transactions on Geoscience and Remote Sensing, Vol.56 , no.3 , pp. 1348 - 1359, March 2018 .

[4] Burkni Palsson, Jakob Sigurdsson, Johannes R. Sveinsson and Magnus O. Ulfarsson, "Hyperspectral Unmixing Using A Neural Network Autoencoder," IEEE Access, Vol. 6, pp. 25646 – 25656, March 2018.

[5] Maoguo Gong, Hao Li, Enhu Luo, Jing Liu and Jia Liu, "A Multi-objective Cooperative Coevolutionary Algorithm for Hyperspectral Sparse Unmixing," IEEE Transactions on Evolutionary Computation , Vol. 21 , no. 2 ,pp. 234 – 248, April 2017.

[6] Yanli Sun, Jose M. BioucasDias2, Xia Zhang1, Yi Liu3 and Antonio Plaza3,"A New Classification Oriented Endmember extraction and Sparse Unmixing approach for Hyperspectral Data," IEEE International Geoscience and Remote Sensing Symposium (IGARSS) ISSN. 2153-7003, pp. 3644 – 364, December 2017.

[7] Rui Wang, Heng-Chao Li, Aleksandra Pizurica, Jun Li, Antonio Plaza, and William J. Emery, "Hyperspectral Unmixing Using Double Reweighted Sparse Regression and Total Variation," IEEE Geoscience and Remote Sensing Letters, Vol. 14, no. 7, pp.1146 – 1150, July 2017.

[8] Rui Wang, Heng-Chao Li, Wenzhi Liao, Xin Huang, and Wilfried Philips, "Centralized Collaborative Sparse Unmixing for Hyperspectral Images," IEEE Journal of Selected Topics in Applied Earth Observations and Remote Sensing, Vol. 10, no. 5, pp. 1949 - 1962, May 2017.

[9] Xiangming Jiang, Maoguo Gong , Hao Li, Mingyang Zhang, and Jun Li, Senior, "A Two-Phase Multiobjective Sparse Unmixing Approach for Hyperspectral Data," IEEE Transactions On Geoscience And Remote Sensing, Vol. 56, no. 1, Jan. 2018.

[10] Yuliya Tarabalka, Mathieu Fauvel, Jocelyn Chanussot, and Jón Atli Benediktsson, "SVM- and MRF-Based Method for Accurate Classification of Hyperspectral Images," IEEE geoscience and remote sensing letters, vol. 7, no. 4, Oct. 2010.

[11] Chein-I Chang, "Hyperspectral Data Exploitation: Theory and Applications," New York: Wiley-Interscience, 2007.

[12] Li, Ting Sun, Kevin F. Kelly and Yin Zhang, "A Compressive Sensing and Unmixing Scheme for Hyperspectral Data Processing Chengbo," IEEE Transactions on Image Processing, Vol. 21, no. 3, pp. 1200 – 1210, Mar. 2012.

[13] Daniel D. Lee and H. Sebastian Seung "Learning the parts of objects by non-negative matrix factorization" Vol. 401, pp. 788–791, Oct. 1999.

[14] Nirmal Keshava and John F. Mustard, "Spectral unmixing," IEEE Signal Processing Magazine, Vol. 19, no.1, pp. 44–57, Jan. 2002.

[15] Si Wang 1, Ting-Zhu Huang , Xi-Le Zhao , Gang Liu and Yougan Cheng, "Double Reweighted Sparse Regression and Graph Regularization for Hyperspectral Unmixing," July, 2018.

[16] A. Tarantola and B. Valette, "Generalized nonlinear inverse problems solved using the least squares criterion," Reviews of

Geophysics.Space Physics, vol. 20, pp. 219-232, May 1982.

[17] J.M.P. Nascimento and J.M.B. Dias," Vertex component analysis: A fast algorithm to unmix hyperspectral data," IEEE Transactions On Geoscience And Remote Sensing, Vol. 43, no. 4 pp. 898–910, April 2005.

[18] Michael E. Winter "N-FINDR: an algorithm for fast autonomous spectral end-member determination in hyperspectral data," Proceedings of SPIE's International Symposium on Optical Science, Engineering, and Instrumentation, Denver, CO, United States, pp. 266–275, Oct. 1999.

[19] Marian-Daniel Iordache, Jose M. Bioucas-Dias and Antonio Plaza, "Total Variation Spatial Regularization for Sparse Hyperspectral Unmixing,"IEEE Transactions on Geoscience and Remote Sensing, Vol. 50, no. 11, pp. 4484–4502, Nov. 2012.

[20] J.M.P. Nascimento and J.M.B. Dias "Does independent component analysis play a role in unmixing hyperspectral data?," IEEE Transactions on Geoscience and Remote Sensing, Vol. 43, no. 1, pp.175–187, Jan. 2005.

[21] Wei He, Hongyan Zhang and Liangpei Zhang, "Sparsity-Regularized Robust Non-Negative Matrix Factorization for Hyperspectral Unmixing," IEEE Journal of Selected Topics in Applied Earth Observations and Remote Sensing , Vol.9, no. 9, pp. 4267 - 4279, Sep. 2016.

[22] Jun Li and Jose M. Bioucas-Dias, "Minimum volume simplex analysis: A fast algorithm to unmix hyperspectral Data,"Proceedings of the IEEE International Geoscience and Remote Sensing Symposium, IGARSS, Boston, MA, USA, 7–11 ,Vol. 3, pp. 250–253, July 2008.

[23] C.-I. Chang, C.-C. Wu, W. Liu and Y.-C. Ouyang, "A New Growing Method for Simplex-Based Endmember Extraction Algorithm" IEEE Transactions on Geoscience and Remote Sensing" Vol. 44, no. 10, pp. 2804–2819, Oct. 2006.

[24] A. Hyvarinen, "Fast and robust fixed-point algorithms for independent component analysis" IEEE Transactions on Neural Networks, Vol. 10, no. 3, pp. 626–634, May 1999.

[25] Gabriel Martin and Antonio Plaza, "Spatial-Spectral Preprocessing Prior to Endmember Identification and Unmixing of Remotely Sensed Hyperspectral Data," IEEE Journal of Selected Topics in Applied Earth Observations and Remote Sensing, Vol. 5, no. 2, pp.380 - 395, Apr. 2012.

[26] Lefei Zhang, Qian Zhang, Bo Du, Xin Huang, Yuan Yan Tang,and Dacheng Tao,"Simultaneous Spectral-Spatial Feature Selection and Extraction for Hyperspectral Images," IEEE Transactions on Cybernetics, Vol. 48 , no. 1 , pp.16 – 28, Jan. 2018.

[27] L. Zhang, X. Zhu, L. Zhang, and B. Du, "Multidomain subspace classification for hyperspectral images," IEEE Trans. Geosci. Remote Sens, vol. 54, no. 10, pp. 6138–6150, Oct. 2016.

[28] Wang, G.G., Deb, S. and Coelho, L.D.S., "Elephant herding optimization," In proceedings of 3rd International Symposium on Computational and Business Intelligence, pp. 1-5, December 2015.

[29] Binu, D. and Kariyappa, B.S., "RideNN: A New Rider Optimization Algorithm-Based Neural Network for Fault Diagnosis in Analog Circuits," IEEE Transactions on Instrumentation and Measurement, 2018.

[30] Urban and Cuprite data, taken from "http://lesun.weebly.com/hyperspectral-data-set.html", accessed on November 2018.

[31] Jun Li ; José M. Bioucas-Dias ; Antonio Plaza ; Lin Liu, " Robust Collaborative Nonnegative Matrix Factorization for Hyperspectral Unmixing", IEEE Transactions on Geoscience and Remote Sensing, vol.54 , no.10, pp. 6076 - 6090, Oct. 2016.

[32] Xu, X. and Shi, Z., "Multi-objective based spectral unmixing for hyperspectral images", ISPRS Journal of Photogrammetry

and Remote Sensing, vol.124, pp.54-69, 2017.

[33] Li, J., Li, H., Liu, Y., & Gong, M. (2021). Multi-fidelity evolutionary multitasking optimization for hyperspectral endmember extraction. Applied Soft Computing, 111, 107713. https://doi.org/10.1016/j.asoc.2021.107713

[34] Wang, Z., Wei, J., Li, J., Li, P., & Xie, F. (2021). Evolutionary multiobjective optimization with endmember priori strategy for large-scale hyperspectral sparse unmixing. Electronics (Switzerland), 10(17), 1–13. https://doi.org/10.3390/electronics10172079

[35] Xu, X., Pan, B., Chen, Z., Shi, Z., & Li, T. (2021). Simultaneously Multiobjective Sparse Unmixing and Library Pruning for Hyperspectral Imagery. IEEE Transactions on Geoscience and Remote Sensing, 59(4), 3383–3395. https://doi.org/10.1109/TGRS.2020.3016941